As GROWTH BANDING AND THE PRESENCE OF Au IN PYRITES FROM THE SANTA RITA GOLD VEIN DEPOSIT HOSTED IN PROTEROZOIC METASEDIMENTS, GOIÁS STATE, BRAZIL

DOMINIQUE MICHEL,

ENSG-CESEV, BP 452, 54001 Nancy, France

GASTON GIULIANI,

ORSTOM and CRPG, BP 20, 54501 Vandoeuvre, France

GEMA RIBEIRO OLIVO,

Université du Québec, Montréal, Québec, Canada H3C 3P8

AND ONILDO JOÃO MARINI

DNPM, 70040 Brasília DF, Brazil

Introduction

Arsenic enrichment in pyrites has been discussed recently for base metal and gold deposits from various geologic environments, such as Carlin-type sediment-hosted gold deposits (Wells and Mullens, 1973) and gold deposits from greenstone belt sequences and carbonate sediments (Fleet et al., 1989). MacLean and Fleet (1989) also observed As growth bandings in pyrites from the Witwatersrand gold fields of South Africa.

As-bearing pyrites are also reported in active geothermal systems. Ballantyne and Moore (1988) have shown that arsenic is erratically distributed in pyrites, with As contents up to 3.8 wt percent, and that arsenopyrite and other As minerals are nearly absent in these systems. Unfortunately, the spatial distribution of As in these pyrites was not investigated.

In a few examples, the oscillatory zonings of As-rich pyrites are related to the enrichment of other traces elements, as in Ni in the Fairview mine (Fleet et al., 1989) and Co in the Witwatersrand gold deposits (MacLean and Fleet, 1989). It is accepted that during pyrite growth these elements coprecipitate with As and are localized in the pyrite lattices.

The identification and distribution of low trace element concentrations (especially gold) in sulfides is a delicate problem which remains unsolved using classical scanning electron microscopy (SEM) and quantitative electron microprobe (QEM) analytical techniques. The studies of Cathelineau et al. (1989) and Marion et al. (1991) on "invisible" gold-bearing sulfides based on data obtained using secondary ion mass spectrometry (SIMS) and [197]Au Mössbauer spectroscopy techniques showed that these sulfides do not contain metallic gold.

In this paper, the study of the Santa Rita gold deposit (gold vein mineralization hosted within Proterozoic metasedimentary formations) reveals interesting features such as typical As-bearing growth bands in pyrite grains. The pyrite grains of the gold mineralization stages are free of detectable native gold. Arsenic-rich oscillatory-zoned pyrites are the only ones to contain invisible gold. The covariations in As and Au indicate that they were transported in the same solution and that the same geochemical processes led to the removal from solution of both.

The Santa Rita Gold Deposit

Regional geology

The Santa Rita gold deposit occurs within the Middle to Upper Proterozoic Paranoá Group (Fig. 1) in the Tocantins province of the Brasília belt located at the western border of the São Francisco craton, Brazil (Marini et al., 1984).

The Paranoá Group consists of two main Proterozoic metasedimentary sequences: the basal units, composed of psammopelites, and the upper units, composed of calcareous psammopelites. The general orientation of the rocks is north-south and they dip 2°-6° W.

Two major faults systems affect the Paranoá Group. The first fault system comprises north-south reverse faults verging eastward. These faults are thrust structures which, to the west, caused overthrusting of Archean and Lower to Middle Proterozoic sequences on top of the Paranoá Group, and to the east, overthrusting of the Paranoá Group on the Upper Proterozoic Bambuí Formation. Some of these thrust structures indicate the boundary of two metamorphic domains in the Paranoá Group—a western domain deformed and metamorphosed in greenschist facies conditions (up to biotite grade) along the lineaments and faults which host gold mineralization, and an eastern domain which is less deformed with very low grade rocks (anchizone).

The second fault system is represented by two northeast-southwest-trending regional lineaments in the western metamorphic domain (Fig. 1). These lin-
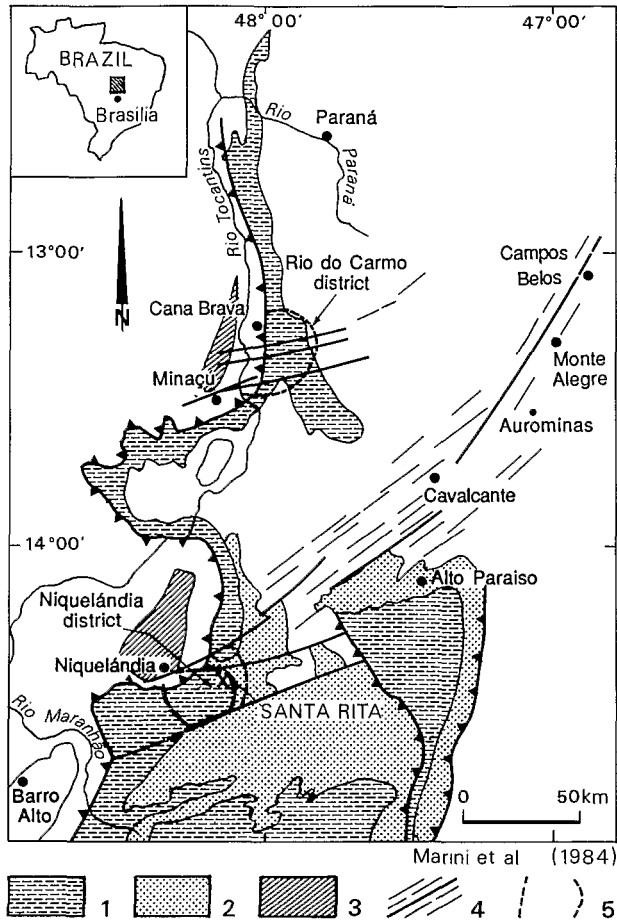
FIG. 1. Geologic setting of the Santa Rita gold occurrence in central Brazil, Goiás State: Paranoá Group, 1 = calcareous psammopelites sequence, 2 = psammopelites sequence, 3 = Niquelandia and Cana Brava basic and ultrabasic massifs, 4 = lineaments and faults, 5 = gold districts.

eaments correspond to older shear zones which crosscut the Niquelandia and Cana Brava Lower Proterozoic basic and ultrabasic massifs (Fig. 1). Gold mineralization is structurally controlled by normal faults and fractures resulting from the reactivation of these older lineaments, and it occurs in two districts: Niquelándia in the south and Rio do Carmo in the north (Fig. 1). These gold districts are located in different stratigraphic horizons of the carbonated psammopelitic sequence and in the uppermost horizons of the psammopelitic sequence.

Olivo et al. (1991) and Giuliani et al. (1993) have proposed a Proterozoic geothermal system model involving the regional thermal gradient for the Paranoá gold deposits. This gradient remained high in the interior of the belt and slowly decreased following the compressive phases of the Brasiliano cycle (Olivo and Marini, 1988).

Local geology

The Santa Rita gold deposit is located in the Niquelándia district and occurs in unit F (Fig. 2) at the base of the calcareous psammopelitic sequence (Olivo, 1989). Unit F was metamorphosed to greenschist grade and consists of a rythmic sequence (F1) of quartzites, carbonaceous quartz phyllites, and muscovite phyllites with lenticular metalimestone and metadolomite, and a sequence (F2) of calcareous phyllites, metalimestone, and metadolomite (Fig. 2).

The primary gold is linked to pyrite-bearing quartz-carbonate veins and veinlets contained at the base of unit F (Fig. 2). The gold veins present a thickness varying from 1 cm to 1 m and a length up to tens of meters. They are structurally controlled by west-northwest–east-southeast high-angle faults, later than the last phase of folding in the Paranoá Group. The gold grades are between 0.1 and 10 ppm, with local values up to 60 ppm.

Paragenetic sequence

The mineralized veins present two stages of formation. In the first stage the faults and fractures were filled by the precipitation of white milky quartz and carbonates. The carbonates are Fe dolomite, ankerite, and calcite which are pigmented by carbonaceous material. A simultaneously restricted hydrothermal alteration is developed in the wall rocks; it is marked by sericitization and albitization of metacarbonates and metadolomites, with an accompanying geochemical enrichment by Co, Ni, and As (Olivo, 1989). The albite occurs as large crystals, often bordered by a sericitic margin. Sericite also occurs disseminated throughout the carbonate rocks or as accidental trapped crystals in fluid inclusion cavities of the quartz.

The second stage is related to the precipitation of clear calcite and auriferous pyrites in veinlets which crosscut the Fe dolomite and ankerite veins. Poikiloblastic calcite and porphyroblastic pyrite occur within the psammitic-pelitic rocks. At this stage no consequent hydrothermal alteration appears and the hydrothermal fluid system wanes.

Pyrites contain rare inclusions of pyrrhotite and chalcopyrite; no visible gold was detected. Pyrites also contain quartz inclusions and, therefore, may have begun to develop contemporeanously or later than some quartz.

Fluid inclusion data

Fluid inclusion studies from the white milky quartz of the pyrite-bearing quartz-carbonate veins were performed by Giuliani et al. (1991, 1993) and Olivo et al. (1991). These studies indicate that the chemical composition of the fluids entering the area of mineralization changed over the period of mineralization.
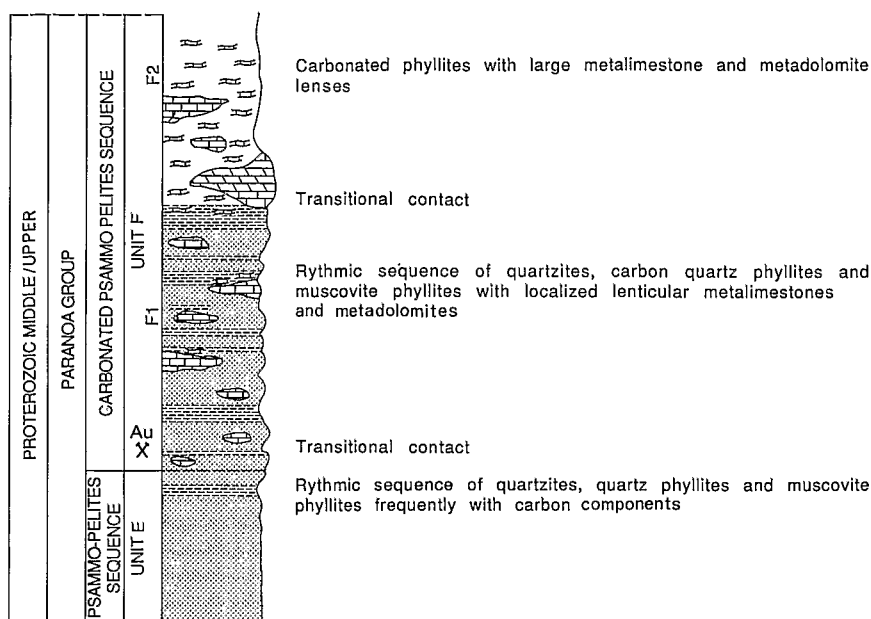
FIG. 2. Lithostratigraphic column of the Paranoá Group with the localization of the Santa Rita gold deposit (from Olivo and Marini, 1988).

These authors cite evidence for two types of fluids —a highly saline, CO_2- and N_2-rich aqueous fluid with halite and sylvite daughter minerals, and a CO_2- and N_2-rich aqueous fluid with moderate to high salinity. These fluids occur in the same quartz crystals and display a great variation in the degree of cavity filling (liquid/vapor ratios) with a dispersion of the microthermometric data. On heating, all of the inclusions decrepitate between 200° and 300°C, prior to homogenization. Raman spectrometry detected high concentrations of N_2 in the gas phase, with CO_2/N_2 ratios between 1 and 19 and a small proportion of CH_4 (up to 2 mole %). The simultaneous entrapment of compositionally variable fluids in the H_2O-CO_2-N_2-NaCl-KCl system enabled Giuliani et al. (1991) and Olivo et al. (1991) to propose a mechanism for mixing of the fluids. They suggested that the entrapment of compositionally variable fluids may result from the mixing of high-salinity fluids with CO_2-N_2 fluids. Considering the absence of spatially and temporally related igneous activity and the very low P-T regional metamorphism in the Paranoá Group, the brines are inferred to be the product of evaporite bed leaching, which occurs in the lower part of the Paranoá lithostratigraphic column.

Analytical Procedures

Scanning electron microscope (SEM) and quantitative electron microprobe (QEM) studies were performed on pyrite crystals. The SEM study was carried out on a Cambridge Stereoscan 250 scanning electron microscope (Université de Nancy I) using the backscattered electron mode, which reveals small differences between average atomic numbers (Z) down to about 0.1. Quantitative electron microprobe (QEM) analyses were performed on a Cameca SX microprobe (Université de Nancy I) using SEM photomicrographs of the Z distribution. The analytical conditions were an accelerating voltage of 30 kV, 60 nA, and a counting time of 30 s for Co, Ni, Ag, Au, and As and 10 s for Fe and S. Fe and S were calibrated with pyrite (Fe: 46.55%, S: 53.43%), As with arsenopyrite (Fe: 33.8%, As: 46.8%, S: 19.4%), and Au, Ag, Co, and Ni with native elements.

The presence of gold was checked further by electron microprobe analyses, performed again with different experimental conditions of 30 kV, 100 nA, and a counting time of 30 min. The detection limit in these conditions is about 70 ppm.

An LMA-10 laser microanalyzer or laser microprobe (ENSG, Nancy) was also used to detect gold in the ore minerals (Schroth, 1972; Butterworth, 1974). Individual grains in polished sections were examined under the microscope prior to and also after the above-mentioned analysis. The intense light energy from the laser was used to excite a spectral emission from the selected pyrite-bearing areas of the samples, with such areas having a minimum diameter of 100 μm. The laser beam vaporized a microgram quantity of the samples, and the vapor was further excited to emit characteristic spectra of the constituent elements.
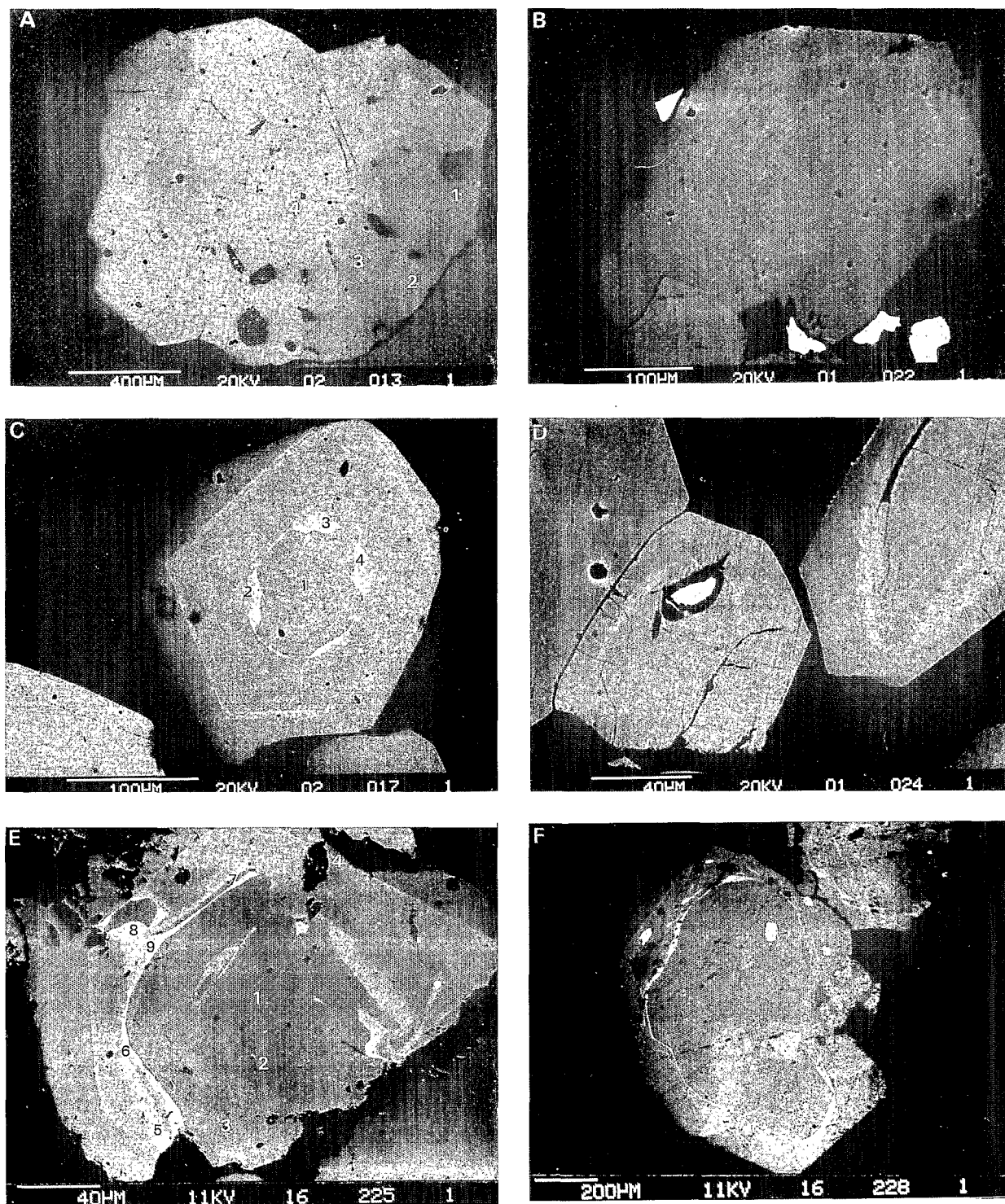
FIG. 3.   Backscattered electron microscopy images showing chemical zonation in pyrite grains (white grains are lead oxides from polishing sample preparation, B, D, F). A. Chemical variations of Ni and Co contents (sample PS7–6a) B. Oscillatory-zoned As-bearing pyrites. The white zones are enriched in As and Co (sample PS7–6b). C. Same as B with well-developed idiomorphic boundaries sometimes enriched by colloformlike structures (sample PS7–6a). D. A single As concentric zoning (sample PS7–6b). E. As growth bands with idiomorphic boundaries and colloformlike structures (sample PS7–6b). F. As zones which are discontinuous in a grain of variable Ni and Co contents (sample PS7–6b). Numbers in A, C, and E correlate with analyses in Table 1.

TABLE 1. Electron Microprobe Analysis (wt %) of Pyrite Grains from Quartz-Carbonate Veins and Veinlets

Sample no.	As	Fe	S	Ni	Co	Total
PS7-6a	0.000	46.463	53.027	0.174	0.000	99.711
PS7-6a (C1)	0.000	46.176	53.099	0.296	0.139	99.787
PS7-6b	0.000	46.084	53.860	0.000	0.216	100.160
PS7-6b	0.000	45.902	53.487	0.000	0.247	99.668
PS7-6a (A1)	0.000	46.297	53.020	0.000	0.256	99.600
PS7-6a (A2)	0.000	46.272	52.975	0.027	0.261	99.558
PS7-6b (E1)	0.000	46.060	53.204	0.000	0.265	99.529
PS7-6b	0.000	45.585	53.803	0.000	0.269	99.669
PS7-6b	0.000	45.708	53.890	0.000	0.284	99.900
PS7-6b (E2)	0.000	45.794	53.250	0.000	0.301	99.353
PS7-6b	0.000	46.164	52.408	0.010	0.337	98.946
PS7-6b	0.000	45.726	54.141	0.029	0.348	100.252
PS7-6b	0.000	45.132	53.440	0.000	0.473	99.068
PS7-6b	0.000	45.253	53.459	0.000	0.706	99.446
PS7-6a (A3)	0.000	45.466	52.912	0.056	1.178	99.619
PS7-6a (A4)	0.000	44.914	52.989	0.084	1.475	99.487
PS7-6b	0.012	45.530	52.658	0.140	1.024	99.364
PS7-6b (E3)	0.037	44.620	53.438	0.075	1.453	99.623
PS7-6b	0.041	45.213	53.627	0.000	0.649	99.538
PS7-6b	0.051	45.675	53.519	0.000	0.252	99.497
PS7-6b	0.058	45.539	53.627	0.058	0.646	99.928
PS7-6b	0.061	45.699	53.625	0.044	0.189	99.618
PS7-6b	0.081	44.548	53.052	0.300	0.903	98.884
PS7-6b	0.081	44.535	53.643	0.161	0.681	99.101
PS7-6b	0.170	45.333	53.607	0.000	0.396	99.506
PS7-6b	0.237	46.215	52.973	0.000	0.210	99.635
PS7-6b	0.357	45.099	53.460	0.000	0.414	99.330
PS7-6a	0.480	46.019	52.455	0.052	0.528	99.534
PS7-6b	0.520	45.321	53.465	0.035	0.320	99.661
PS7-6b (E4)	0.547	45.368	53.719	0.053	0.420	100.107
PS7-6b	0.549	45.539	53.207	0.057	0.249	99.601
PS7-6b	0.632	45.690	52.965	0.112	0.510	99.909
PS7-6a (C2)	0.835	45.580	52.450	0.035	0.909	99.809
PS7-6a (C3)	0.933	44.979	52.251	0.000	1.743	99.910
PS7-6b	1.031	44.266	53.003	0.000	1.126	99.433
PS7-6b	1.088	44.705	53.174	0.061	1.071	100.099
PS7-6b	1.099	44.296	53.302	0.000	1.369	100.066
PS7-6b	1.147	44.616	52.968	0.022	1.161	99.914
PS7-6b	1.176	44.588	52.830	0.078	1.142	99.814
PS7-6b	1.192	44.296	52.594	0.091	1.133	99.306
PS7-6b	1.399	44.381	52.623	0.081	1.300	99.784
PS7-6b	1.437	44.238	52.692	0.063	1.224	99.654
PS7-6b	1.443	44.534	52.192	0.370	0.550	99.089
PS7-6b	1.565	45.145	52.361	0.422	0.391	99.884
PS7-6b	1.882	44.330	52.435	0.512	0.395	99.554
PS7-6b (ES)	1.928	44.184	51.743	0.000	1.894	99.749
PS7-6b	2.089	44.865	51.900	0.557	0.416	99.827
PS7-6b	2.201	42.534	52.675	0.000	2.258	99.668
PS7-6b (E6)	2.448	43.060	51.553	0.000	2.480	99.541
PS7-6b	2.588	43.683	51.635	0.000	2.482	100.39
PS7-6b	2.622	43.245	51.469	0.000	2.587	99.923
PS7-6b (E7)	2.669	42.866	51.588	0.000	2.369	99.492
PS7-6b	3.044	42.193	51.569	0.000	2.921	99.727
PS7-6b (E8)	3.066	41.930	51.290	0.000	3.133	99.419
PS7-6b (E9)	3.837	41.877	50.918	0.000	3.526	100.158
PS7-6a (C4)	4.185	41.732	49.850	0.000	4.094	99.880

Analyses are presented according to increasing As concentrations; detection limits for a counting time of 30 s are Co-150 ppm, Ni-135 ppm, As-335 ppm (the values under the detection limits are set to zero); each analysis which corresponds to localized points in Figure 3 is noted with the letter of the photos (A, C, or E) and the same number in the photos
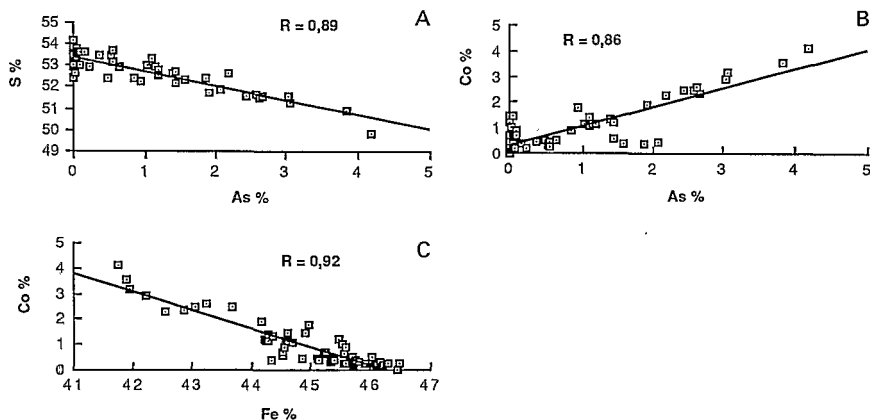
FIG. 4.   Correlation curves in the pyrite grains from veins and veinlets. Analyses are from Table 1. A. Inverse correlation between As and S. B. Positive correlation between As and Co. C. Inverse correlation between Fe and Co. Percent = wt percent concentrations.

The element content data were semiquantitative and were obtained by comparison with the spectra performed on standard samples of pyrites containing different, known, introduced gold concentrations. The sizes of the craters resulting from the laser beams in the standards and the examined samples of pyrites must be identical in order for the same amount of substance to be tested in both.

Each standard sample of pyrite was prepared by mixing variably measured concentrations of ultra finely crushed $NaAuCl_4 \cdot 2H_2O$ and pure pyrite in an agate mortar for 2 h and then making a pellet with a pressing machine. Statistically, the mixing of these ultra finely crushed products will give a uniform Au content in the pyrites which can be confirmed by several laser microprobe analyses. The standards of pyrites obtained contain 1 percent, 3,160, 1,000, 316, and 100 ppm of homogeneously distributed gold.

Results

Chemical compositions of the pyrites

Chemical variations in the pyrite grains detected by SEM and QEM analyses allowed the identification of two groups of pyrites. They are spatially associated but without clear textural relationships.

The first group shows variable concentrations of cobalt and nickel without any detectable As (Fig. 3A). In such grains, Co and Ni contents may vary from 0 to 1.47 and 0 to 0.30 wt percent, respectively (Table 1).

The second group typically displays As enrichments (Fig. 3B–F) in oscillatory-zoned pyrites which are bounded by scarce grains of chalcopyrite and
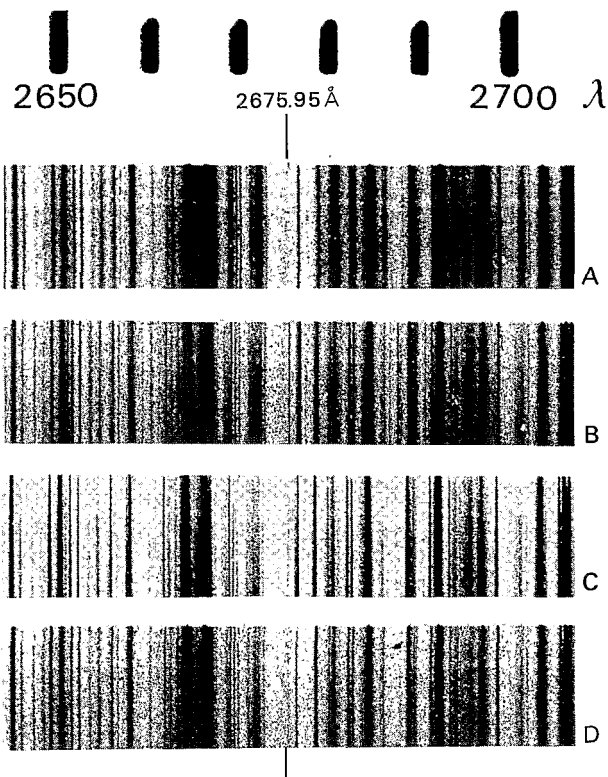

FIG. 5.   Laser microprobe spectrums with the characteristic gold emission line at 2675.95 Å. A. Spectrum of spectrographic quality iron. B. Standard spectrum of pyrite with 316 ppm Au (see text "Analytical procedures" for explanation). C. Standard spectrum of pyrite with 100 ppm Au. D. Santa Rita As growth-bandings pyrite (sample PS7–6a). The presence of the gold emission line is obvious with an estimate concentration of 100 ppm by comparison with the standards spectrums.

pyrrhotite that are a few microns in size ($\pm 5 \times 10$ μm). The As zones are indicated by the presence of white-colored zones under the backscattered electron microprobe mode (Fig. 3B-F). Some As-rich zones show euhedral boundaries subparallel to the crystal faces, which are sometimes complicated by colloform structures (Fig. 3C and E) and are often concentric. The succession of different As zones gives the appearance of typical oscillatory-zoned pyrites (Fig. 3B, C, and E). Other As zones do not show any idiomorphic boundaries, present variable widths, are sometimes discontinuous, and are not repeated in the pyrite grains (Fig. 3D and F).

The As contents of the As-bearing zones vary between 0.04 to 4.18 wt percent (Table 1). In each well-defined zone, the As content is quite uniform. A clear inverse correlation exists between arsenic and sulfur (Fig. 4A). The As enrichments are also closely correlated with Co enrichments up to 4.09 percent (Fig. 4B). Other than in the As zones, the Co contents are up to 1.47 percent (Table 1). Furthermore, an inverse correlation exists between Co and Fe (Fig. 4C).

Gold in the pyrites

In the Santa Rita deposit, pyrite exploitation by prospectors and chemical analyses of the ore has shown that gold is spatially associated with pyrite.

Native gold was not detected using conventional and scanning electron microscopic studies. The occurrence of gold in the pyrite was therefore investigated by an electron microprobe and LMA-10 laser microprobe.

The electron microprobe study was inconclusive. The LMA-10 laser microprobe studies were performed on both the As oscillatory zoned and unzoned pyrites. The latter do not contain any gold but about 100 ppm of gold was detected in the former (Fig. 5).

Interpretations

The textural observations obviously indicate that the As-rich zones occur more or less as concentric zones in the pyrite grains. The development of idiomorphic boundaries and the localization of a few pyrrhotite and chalcopyrite grains at the limits of As-rich zones inside the pyrites argue for crystal growth processes. The arsenic-rich zones are As growth bandings of the pyrites grains.

From a mineralogical point of view, there are several possible origins of these As growth bandings. The first is the presence of As-bearing minerals as cryptoinclusions. Considering the electron microprobe analyses, these As-bearing minerals would be of an AX_2 type, with two ligands for one metal, and would contain cobalt (Co shows a positive correlation with As). These minerals could be either pyrite isotypic minerals such as cobaltite (CoAsS) or marcasite

isotypic minerals such as safflorite (CoAs$_2$), loellingite (FeAs$_2$), and arsenopyrite (FeAsS). The last two minerals often contain Co atoms in the Fe sites of their lattices.

The second possibility is the presence of As and Co substituting for S and Fe, respectively, in the pyrite lattice based on the inverse correlations As/S and Co/Fe. These substitutions should induce some changes in the crystalline lattice parameters. Fleet et al. (1989), based on transmission electron microscopy (TEM) and X-ray diffraction data, concluded that As is incorporated in pyrite as a metastable solid solution of the Fe (S, As)$_2$ type, with a marcasitelike structure.

The only pyrites of the Santa Rita gold deposit that contain gold show As-rich growth bands. Marion et al. (1991) investigated the gold status in similar As-zoned pyrites using [197]Au Mössbauer spectrometry. They concluded that the gold is not metallic or chemically connected with Au-rich arsenopyrite cryptoinclusions but rather is bound within pyrite as atoms in the lattice (possibly in an interstitial position or substitution sites) or as cryptoinclusions of a gold-rich phase.
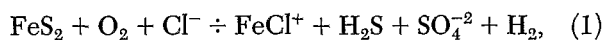
The geochemical association of As-bearing sulfides and Au is well established. In the Santa Rita deposit, the As-bearing zones are also enriched in Co. As seen above, these can correspond to different mineralogical occurrences that still need to be elucidated, especially by transmission electron microscope (TEM) and X-ray microdiffraction studies. However, problems in the localization of As-Au-rich zones under a microscope electron beam are of critical importance for a correct interpretation of diffraction patterns (Marion, 1988).

In the Santa Rita deposit, the fluids (H$_2$O-CO$_2$-N$_2$-NaCl-KCl from fluid inclusion data) moved in a single hydrothermal system linked to the existence of a regional Proterozoic geothermal system as proposed by Olivo and Marini (1988) and Olivo et al. (1991).
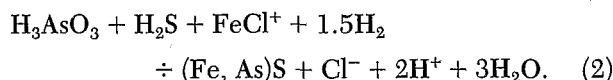
The pyrite grains with clear calcite appear to be the latest minerals which precipitated in the veins. The presence of colloformlike structures of some pyrite As-rich zones (Fig. 3C and E) indicates relatively low-temperature formation. Such As- and trace element-rich pyrite tends to form in low-temperature hydrothermal systems (Wells and Mullins, 1973; Fleet et al., 1989). The covariations in As and Au indicate that they were transported in the same solution and that the same geochemical processes led to the destabilization from solution of both. There are no available data about possible arsenic-gold complexes.

The arsenic geochemistry in actual geothermal systems has been studied by Ballantyne and Moore (1988). In many geothermal reservoirs, pH and PO_2 are close to the pyrite-hematite boundary. The predominant As species is H$_3$AsO$_3$. The authors have

concluded that local microscale irreversible reactions explain the occurrence of As in pyrite in geothermally altered rocks. They have proposed that the oxidation of one part of a pyrite grain (eq 1) may in turn lead to low P_{O_2} and high P_{H_2} in another part of the grain (eq 2).

$$FeS_2 + O_2 + Cl^- \div FeCl^+ + H_2S + SO_4^{-2} + H_2, \quad (1)$$

and

$$H_3AsO_3 + H_2S + FeCl^+ + 1.5H_2$$
$$\div (Fe, As)S + Cl^- + 2H^+ + 3H_2O. \quad (2)$$

In the Santa Rita deposit, the pyrite grains are the latest minerals in the vein fillings related to the progressive decreasing of regional thermal gradients and the consequent closing of the hydrothermal circulation. Fluctuations in redox conditions are probable in an overall waning hydrothermal fluid system and may cause the formation of the As growth bandings of the pyrites in a way similar to that described above.

The available known gold complexes in actual geothermal systems are $AuCl_2^-$ or $Au(HS)_2^-$ (Benedetti, 1989; Seward, 1989). The gold mineralogical nature of As-bearing pyrites is still unknown, but it is known that fluctuations in redox conditions would generate changes in the stability of gold complexes and the cofixation with As-rich pyrites.

Acknowledgments

November 8, 1991; June 17, 1993

REFERENCES

Ballantyne, J.M., and Moore, J.N., 1988, Arsenic geochemistry in geothermal systems: Geochimica et Cosmochimica Acta, v. 52, p. 475–483.

Bénedetti, M., 1989, Géochimie de l'or, mécanismes de transport et de dépôt: Unpublished Ph.D., l'Université de Paris VII, 197 p.

Butterworth, A., 1974, Laser microspectral analyser: Forensic Science Society Journal, v. 14, 123 p.

Cathelineau, M., Boiron, M.C., Holliger, P., Marion, P., and Denis, M., 1989, Gold-rich arsenopyrites: Crystal chemistry, gold location and state, physical chemical conditions of crystallization: ECONOMIC GEOLOGY MONOGRAPH 6, p. 328–341.

Fleet, M.E., MacLean, P.J., and Barbier, J., 1989, Oscillatory-zoned As-bearing pyrite from strata-bound and stratiform gold deposits: An indicator of ore fluid evolution: ECONOMIC GEOLOGY MONOGRAPH 6, p. 356–362.

Giuliani, G., Fortes, P.T., Nilson, A.A., Dardenne, M.A., Olivo, G.R., Ronchi, L.H., Santos, M.M., and Marini, O.J., 1991, Contrasting Archean-Proterozoic-hosted gold deposit types and associated gold-bearing fluids, in Pagel, M., and Leroy, J.L., eds., Source, transport and deposition of metals: Rotterdam, A.A. Balkema, p. 665–668.

Giuliani, G., Olivo, G.R., Marini, O.J., and Michel, D., 1993, The Santa Rita gold deposit in the Proterozoic Paranoá Group, Goias, Brazil: An example of fluid mixing during ore deposition: Ore Geology Reviews, v. 8, p. 503–523.

MacLean, P.J., and Fleet, M.E., 1989, Detrital pyrite in the Witwatersrand gold fields of South Africa: Evidence from truncated growth banding: ECONOMIC GEOLOGY, v. 84, p. 2008–2011.

Marini, O.J., Fuck, R.A., Dardenne, M.A., and Danni, J.C.M., 1984, Provincia Tocantins: Setores Central e Sudeste, in Almeida, F.F.M., and Hasui, Y., eds., O Precambriano do Brasil: São Paulo, Edgar Blücher Ltda., p. 205–264.

Marion, P., 1988, Caractérisation de minerais sulfurés aurifères, mise en oeuvre de méthodes classiques et nouvelles: Thése Sciences Physiques, INPL, Nancy, France, 401 p.

Marion, P., Monroy, M., Holliger P., Boiron, M.C., Cathelineau, M., Wagner, F.E., and Friedl, J., 1991, Gold bearing pyrites: A combined ion microprobe and Mössbauer spectrometry approach, in Pagel, M., and Leroy, J.L., eds., Source, transport and deposition of metals: Rotterdam, A.A. Balkema, p. 677–680.

Olivo, G.R., 1989, Controle litoestratigráfico e gênese das occorências auriferas da sequência psamo-pelito-carbonática do grupo Paranoá-Go: Unpublished M.Sc. thesis, Universidad da Brasilia, Brazil, 400 p.

Olivo, G.R., and Marini, O.J., 1988, Ouro no Grupo Paranoá: Distribuição, tipos e contrôles dos ocorrenciãs: Congresso Brasileiro de Geologia, 35th, Belem, v. 1, p. 93–106.

Olivo, G.R., Marini, O.J., and Giuliani G., 1991, Hydrothermal gold occurrences hosted by Middle to Upper Proterozoic carbonate sequence: The example of the Santa Rita prospect, Goiás, Brazil, in Ladeira, E.A., ed., Gold '91: Rotterdam, A.A. Balkema, p. 339–341.

Schroth, H., 1972, Quantitative laser-mikrospektralanalyse verschiedener materialien im ungesteuerten und gütegesteuerten laserbetrieb: Zeitschrift für Analytische Chemie, v. 261, 21 p.

Seward, T.M., 1989, The hydrothermal chemistry of gold and its implications for ore formation: Boiling and conductive cooling as examples: ECONOMIC GEOLOGY MONOGRAPH 6, p.398–404

Wells, J.D., and Mullens, T.E., 1973, Gold-bearing arsenian pyrite determined by microprobe analysis, Cortez and Carlin Gold mines, Nevada: ECONOMIC GEOLOGY, v. 68, p. 187–201.